

# Measurement of Strange-Quark Contributions to the Nucleon's Form Factors at $Q^2 = 0.230$ (GeV/c) $^2$

F. E. Maas,<sup>1,\*</sup> P. Achenbach,<sup>1</sup> K. Aulenbacher,<sup>1</sup> S. Baunack,<sup>1</sup> L. Capozza,<sup>1</sup> J. Diefenbach,<sup>1</sup> K. Grimm,<sup>1</sup> Y. Imai,<sup>1</sup> T. Hammel,<sup>1</sup> D. von Harrach,<sup>1</sup> E.-M. Kabuß,<sup>1</sup> R. Kothe,<sup>1</sup> J. H. Lee,<sup>1</sup> A. Lorente,<sup>1</sup> A. Lopes Ninja,<sup>1</sup> L. Nungesser,<sup>1</sup> E. Schilling,<sup>1</sup> G. Stephan,<sup>1</sup> C. Weinrich,<sup>1</sup> I. Altarev,<sup>2</sup> J. Arvieux,<sup>3</sup> B. Collin,<sup>3</sup> R. Frascaria,<sup>3</sup> M. Guidal,<sup>3</sup> R. Kunne,<sup>3</sup> D. Marchand,<sup>3</sup> M. Morlet,<sup>3</sup> S. Ong,<sup>3</sup> J. van de Wiele,<sup>3</sup> S. Kowalski,<sup>4</sup> B. Plaster,<sup>4</sup> R. Suleiman,<sup>4</sup> and S. Taylor<sup>4</sup>

<sup>1</sup>*Institut für Kernphysik, Johannes Gutenberg Universität Mainz, J. J. Becherweg 45, D-55099 Mainz, Germany*

<sup>2</sup>*St. Petersburg Institute of Nuclear Physics, Gatchina, Russia*

<sup>3</sup>*Institut de Physique Nucléaire, 91406 Orsay Cedex, France*

<sup>4</sup>*Laboratory for Nuclear Science, Massachusetts Institute of Technology, Cambridge, Massachusetts 02139, USA*

(Received 11 December 2003; published 7 July 2004)

We report on a measurement of the parity-violating asymmetry in the scattering of longitudinally polarized electrons on unpolarized protons at a  $Q^2$  of 0.230 (GeV/c) $^2$  and a scattering angle of  $\theta_e = 30^\circ$ – $40^\circ$ . Using a large acceptance fast PbF<sub>2</sub> calorimeter with a solid angle of  $\Delta\Omega = 0.62$  sr, the A4 experiment is the first parity violation experiment to count individual scattering events. The measured asymmetry is  $A_{\text{phys}} = (-5.44 \pm 0.54_{\text{stat}} \pm 0.26_{\text{sys}}) \times 10^{-6}$ . The standard model expectation assuming no strangeness contributions to the vector form factors is  $A_0 = (-6.30 \pm 0.43) \times 10^{-6}$ . The difference is a direct measurement of the strangeness contribution to the vector form factors of the proton. The extracted value is  $G_E^s + 0.225G_M^s = 0.039 \pm 0.034$  or  $F_1^s + 0.130F_2^s = 0.032 \pm 0.028$ .

DOI: 10.1103/PhysRevLett.93.022002

PACS numbers: 13.60.Fz, 11.30.Er, 12.15.-y, 13.40.Gp

The understanding of sea-quark degrees of freedom of the nucleon in the nonperturbative regime of quantum chromodynamics is very poor even today. Since the nucleon has no net strangeness, any contribution of strange quarks to the nucleon structure observables is a pure sea-quark effect. For example, the scalar strangeness content of the nucleon that gives a contribution to the mass of the nucleon has been discussed in the context of the  $\Sigma$  commutator, which can be related to the  $\pi$ - $N$  scattering amplitude [1]. The interpretation of the nucleon spin content results [2] suggests a sizeable contribution,  $\Delta s = -10 \pm 10\%$ , of the strange quarks to the nucleon spin.

Estimates of the strange quark contribution to the magnetic and electric vector form factors predict sizable effects accessible to experiments [3,4]. Recently, two experiments [5,6] have explored parity-violating (PV) asymmetries on the proton and the deuteron in two different kinematical regions. We report here on a new measurement at a four momentum transfer  $Q^2$  of 0.230 (GeV/c) $^2$  at the Mainzer Mikrotron accelerator facility (MAMI) [7]. The A4 experiment at MAMI is complementary to other experiments for two reasons. First, its  $Q^2$  value tests models predicting an enhanced strangeness contribution [8] and second, for the first time counting techniques are used in a scattering experiment measuring a PV asymmetry. Therefore, possible systematic contributions to the experimental asymmetries and the associated uncertainties are of a different nature as compared to previous experiments, which use analogue integrating techniques.

Access to the strangeness nucleon vector current matrix elements is possible by a measurement of the weak vector

form factors  $\tilde{G}_{E,M}^p$  of the proton [9]. They can be expressed in terms of the known nucleon electromagnetic vector form factors  $G_{E,M}^{p,n}$  and the unknown strangeness contribution  $G_{E,M}^s$ . The interference between weak ( $Z^0$ ) and electromagnetic ( $\gamma$ ) amplitudes leads to a PV asymmetry  $A_{LR}(\vec{e}p)$  in the elastic scattering cross section for right- and left-handed electrons ( $\sigma_R$  and  $\sigma_L$ , respectively), which is given in the framework of the standard model [10] and can be expressed as a sum of three terms,  $A_{LR}(\vec{e}p) = A_V + A_s + A_A$ , with

$$A_V = -a\rho'_{\text{eq}} \left\{ (1 - 4\hat{\kappa}'_{\text{eq}}\hat{s}_Z^2) - \frac{\epsilon G_E^p G_E^n + \tau G_M^p G_M^n}{\epsilon(G_E^p)^2 + \tau(G_M^p)^2} \right\}, \quad (1)$$

$$A_s = a \left\{ \rho'_{\text{eq}} \frac{\epsilon G_E^p G_E^s + \tau G_M^p G_M^s}{\epsilon(G_E^p)^2 + \tau(G_M^p)^2} \right\}, \quad (2)$$

$$A_A = a \left\{ \frac{(1 - 4\hat{s}_Z^2)\sqrt{1 - \epsilon^2}\sqrt{\tau(1 + \tau)}G_M^p \tilde{G}_A^p}{\epsilon(G_E^p)^2 + \tau(G_M^p)^2} \right\}. \quad (3)$$

$A_V$  represents the vector coupling on the proton vertex where the possible strangeness contribution has been taken out and has been put into  $A_s$ , a term arising only from a contribution of strangeness to the electromagnetic vector form factors. The term  $A_A$  represents the contribution from the axial coupling at the proton vertex due to the neutral current weak axial form factor  $\tilde{G}_A^p$ . The quantity  $a$  represents  $(G_\mu Q^2)/(4\pi\alpha\sqrt{2})$ .  $G_\mu$  is the Fermi coupling constant as derived from muon decay.  $\alpha$  is the fine structure constant,  $Q^2$  the negative square of the four momentum transfer,  $\tau = Q^2/(4M_p^2)$ , with  $M_p$  the proton mass, and  $\epsilon = [1 + 2(1 + \tau) \times \tan^2(\theta_e/2)]^{-1}$ , with  $\theta_e$  the

laboratory scattering angle. The electromagnetic form factors  $G_{E,M}^{p,n}$  are taken from a recent parameterization (version 1, page 5) by Friedrich and Walcher [11], where we assign an experimental error of 3 % to  $G_M^p$  and  $G_E^p$ , 5 % to  $G_M^n$ , and 10 % to  $G_E^n$ . Electroweak radiative corrections are included in the factors  $\rho'_{\text{eq}}$  and  $\hat{\kappa}'_{\text{eq}}$ , which have been evaluated in the  $\overline{MS}$  renormalization scheme [12]. We use a value for  $\hat{s}_Z^2 = \sin^2 \theta_W (M_Z)_{\overline{MS}}$  of 0.23113(15) [13]. The electroweak radiative corrections to  $A_A$  (Ref. [14]) as well as a value of  $\Delta s = -0.1 \pm 0.1$  are included in  $\tilde{G}_A$ . Electromagnetic internal and external radiative corrections to the asymmetry and the effect of energy loss due to ionization in the target have been calculated. They reduce the expected asymmetry in our kinematics by about 1.3 %. We average  $A_0 = A_V + A_A$  over an acceptance of the detector and the target length. We obtain the expected value for the asymmetry at the averaged  $Q^2$  without strangeness contribution to the vector form factors of  $A_0[Q^2 = 0.230 \text{ (GeV/c)}^2] = -6.30 \pm 0.43$  ppm.

The PV asymmetry was measured at the MAMI accelerator facility in Mainz [7] using the setup of the A4 experiment [15]. The polarized 854.3 MeV electrons were produced using a strained layer GaAs crystal that is illuminated with circularly polarized laser light [16]. Average beam polarization was about 80 %. The helicity of the electron beam was selected every 20.08 ms by setting the high voltage of a fast Pockels cell according to a pattern of four helicity states, either  $(+P - P - P + P)$  or  $(-P + P + P - P)$ . The pattern was selected randomly by a pseudorandom bit generator. A 20 ms time window enabled the histogramming in all detector channels and an integration circuit in the beam monitoring and luminosity monitoring systems. For normalization, the gate length was measured for each helicity. Between each 20 ms measurement gate, there was an 80  $\mu\text{s}$  time window for the high voltage at the Pockels cell to be changed. The intensity  $I = 20 \mu\text{A}$  of the electron current was stabilized to better than  $\delta I/I \approx 10^{-3}$ .

We have used a system of microwave resonators in order to monitor beam current, energy, and position in two sets of monitors separated by a drift space of about 7.21 m in front of the hydrogen target. In addition, we have used a system of ten feedback loops in order to stabilize current, energy [17], position, and angle of the beam. The polarization of the electron beam was measured using a Møller polarimeter with an accuracy of 2.1 % [18], which is located on a beam line in another experimental hall. Because of the fact that we had to interpolate between the weekly Møller measurements, the uncertainty in the knowledge of the beam polarization increased to 4 %. The 10 cm high power, high flow liquid hydrogen target was optimized to guarantee a high degree of turbulence with a Reynolds number of  $Re > 2 \times 10^5$  in the target cell in order to increase the effective heat transfer. For the first time, a fast modulation of the beam position of the intense cw 20  $\mu\text{A}$  beam and stabilization of the beam position on the target cell without

target density fluctuations arising from boiling could be avoided. The total thickness of the entrance and exit aluminum windows was 250  $\mu\text{m}$ . The luminosity  $L$  was monitored for each helicity state ( $R, L$ ) during the experiment using eight water-Cerenkov detectors (LuMo) that detect scattered particles symmetrically around the electron beam for small scattering angles in the range of  $\theta_e = 4^\circ - 10^\circ$ , where the PV asymmetry is negligible. The photomultiplier tube currents of these luminosity detectors were integrated during the 20 ms measurement period by gated integrators and then digitized by customized 16-bit analogue-to-digital converters (ADC). The same method was used for all the beam parameter signals. A correction was applied for the nonlinearity of the luminosity monitor photomultiplier tubes. This was measured and verified separately by varying the beam current from 0–23  $\mu\text{A}$  several times per week. From the beam current helicity pair data  $I^{R,L}$  and luminosity monitor helicity pair  $L^{R,L}$  data, we calculated the target density  $\rho^{R,L} = L^{R,L}/I^{R,L}$  for the two helicity states independently.

To detect the scattered electrons, we developed a new type of a very fast, homogeneous, total absorption calorimeter consisting of individual lead fluoride ( $\text{PbF}_2$ ) crystals [19,20]. This is the first time this material has been used in a large scale calorimeter for a physics experiment. Together with the readout electronics, this allows us a measurement of the particle energy with a resolution of  $3.9\%/\sqrt{E}$  and a total deadtime of 20 ns. At the time of the data taking, 511 out of 1022 channels of the detector and the readout electronics were operational. The detector modules were located in two sectors covering an azimuthal angle interval  $\Delta\phi$  of  $90^\circ$  symmetrically around the beam axis. The particle rate within the acceptance of this solid angle was  $\approx 50 \times 10^6 \text{ s}^{-1}$ . Because of the short deadtime, the losses due to double hits in the calorimeter were 1 % at 20  $\mu\text{A}$ . The signals from each cluster of nine crystals were summed and integrated for 20 ns in an analogue summing and triggering circuit and digitized by a transient 8-bit ADC. There was one summation, triggering, and digitization circuit per crystal. The energy, helicity, and impact information were stored together in a three-dimensional histogram. Figure 1 shows a typical energy spectrum of scattered particles from the hydrogen target at an electron current of 20  $\mu\text{A}$ . It was taken during 5 min and is a direct output of the histogramming memory. The elastic scattering peak is clearly isolated at the high end of the spectrum.

The number of elastic scattered electrons is determined for each detector channel by integrating the number of events in an interval from  $1.6\sigma_E$  above pion production threshold to  $2.0\sigma_E$  above the elastic peak in each helicity histogram, where  $\sigma_E$  is the energy resolution for nine crystals. These cuts ensure a clean separation between elastic scattering and pion production or  $\Delta$  excitation, which has an unknown PV cross section asymmetry. We determined the number of elastically scattered electrons

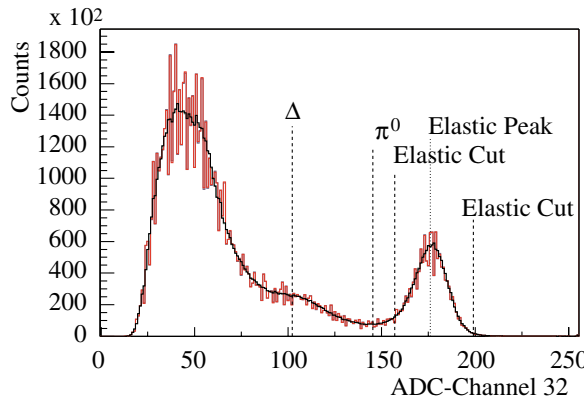


FIG. 1 (color online). The dashed histogram shows a raw energy spectrum of accepted particles from the hydrogen target as read directly from the hardware memory of the readout electronics of the lead fluoride calorimeter. For the solid black curve, this raw spectrum has been corrected for the differential nonlinearity of the ADC, i.e., for measured variations of the ADC channel width. The position of the elastic scattering peak, the threshold for  $\pi^0$  production, and the position of the  $\Delta$  resonance is indicated as well as the lower and the upper cut positions for the extraction of  $N_e^R$  and  $N_e^L$  as described in the text.

for each helicity state ( $N_e^R$  and  $N_e^L$ ) by summing over the inner 345 detector channels, which are the centers of a full  $3 \times 3$  crystal matrix. The linearity of the  $\text{PbF}_2$  detector system with respect to particle counting rates and possible effects due to deadtime were investigated by varying the beam current. We calculate the raw normalized detector asymmetry as  $A_{\text{raw}} = (N_e^R/\rho^R - N_e^L/\rho^L)/(N_e^R/\rho^R + N_e^L/\rho^L)$ . The possible dilution of the measured asymmetry by background originating from the production of  $\pi^0$ 's that subsequently decays into two photons where one of the photons carries almost the full energy of an elastic scattered electron was estimated using Monte Carlo simulations to be much less than 1% and is neglected here. The largest background comes from quasi-elastic scattering at the thin aluminum entrance and exit windows of the target cell (Table I).

Corrections due to false asymmetries arising from helicity correlated changes of beam parameters were applied on a run by run basis. The analysis was based on the 5 min runs for which the counted elastic events in the  $\text{PbF}_2$  detector were combined with the correlated beam parameter and luminosity measurements. In the analysis we applied reasonable cuts in order to exclude runs where the accelerator or parts of the  $\text{PbF}_2$  detector system were malfunctioning. The analysis is based on a total of  $7.3 \times 10^6$  histograms corresponding to  $4.8 \times 10^{12}$  elastic scattering events.

We extracted an experimental asymmetry from  $A_{\text{exp}} = A_{\text{raw}} - a_1 A_I - a_2 \Delta x - a_3 \Delta y - a_4 \Delta x' - a_5 \Delta y' - a_6 \Delta E_e$ . The six  $a_i$  ( $i = 1 \dots 6$ ) denote the correlation coefficients between the observed false asymmetry and the electron current asymmetry  $A_I$ , the horizontal and vertical beam position differences  $\Delta x$ ,  $\Delta y$ , the horizontal and vertical

TABLE I. Overview of the applied corrections and the sources of the experimental error in the measured asymmetry.

	Correction [ppm]	Error [ppm]
Statistics		0.54
Target density, luminosity	0.58	0.09
Target density, beam current	0.00	0.04
Nonlinearity of LuMo	0.30	0.04
Deadtime correction	-0.11	0.08
$A_I$	0.64	0.04
$\Delta E_e$	-0.05	0.02
$\Delta x$ , $\Delta y$	-0.03	0.02
$\Delta x'$ , $\Delta y'$	0.03	0.03
Aluminum windows ( $\text{H}_2$ target)	0.16	0.02
Dilution from $\pi^0$ decay	0.00	0.06
$P_e$ measurement	-1.07	0.11
$P_e$ interpolation	0.00	0.19
Systematic error		0.26

beam angle differences  $\Delta x'$ ,  $\Delta y'$ , and the beam energy difference  $\Delta E_e$ . For the analysis, the correlation parameters  $a_i$  were extracted by multidimensional regression analysis from the data. The  $a_i$  have been calculated in addition from the geometry of the precisely surveyed detector geometry. The two different methods agree very well within statistics.

The experimental asymmetry was normalized to the electron beam polarization  $P_e$  to extract the physics asymmetry,  $A_{\text{phys}} = A_{\text{exp}}/P_e$ . We have taken half of our data with a second  $\lambda/2$  plate inserted between the laser system and the GaAs crystal. This reverses the polarization of the electron beam and allows a stringent test of the understanding of systematic effects. The effect of the plate can be seen in Fig. 2: the observed asymmetry extracted from the different data samples changes sign, which is a clear sign of parity violation. Our measured result for the PV physics asymmetry in the scattering cross section of polarized electrons on unpolarized protons at an average  $Q^2$  value of 0.230 ( $\text{GeV}/c$ )<sup>2</sup> is  $A_{\text{phys}} = (-5.44 \pm 0.54 \pm 0.26)$  ppm. The first error represents the statistical accuracy, and the second error represents the systematical uncertainties including beam polarization. The absolute accuracy of the experiment represents the most accurate measurement of a PV asymmetry in the elastic scattering of longitudinally polarized electrons on unpolarized protons. Table I gives an overview of the applied corrections.

The interpretation of the measurement in terms of strangeness contribution is possible by comparing the measured physics asymmetry  $A_{\text{phys}}$  with the averaged theoretical value without strangeness contribution  $A_0$ . The difference  $A_{\text{phys}} - A_0$  is proportional to an averaged combination of the Sachs form factors  $G_E^s + 0.225G_M^s = 0.039 \pm 0.034$ . If one uses the Dirac and Pauli form factors instead, the extracted value is  $F_1^s + 0.130F_2^s = 0.032 \pm 0.028$ . The solid line in Fig. 3 illustrates the

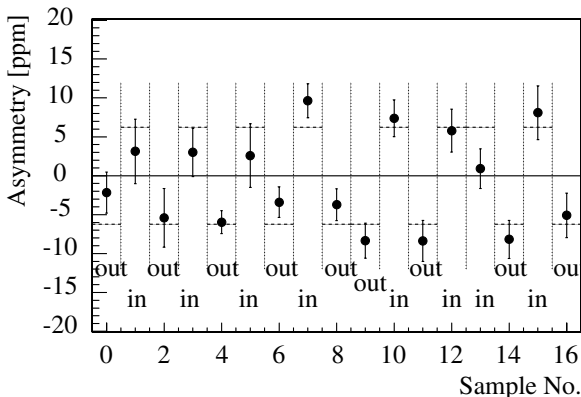


FIG. 2. The extracted experimental asymmetries are shown with the  $\lambda/2$  plate in or out, respectively, as a function of the data sample. The dashed line represents the value of  $A_0$  as described in the text.

possible combinations of  $G_E^s$  and  $G_M^s$  given by our result. The measured combination is small and is 1.2 standard deviations away from zero, which clearly rules out the pole fit type of theoretical models on the strangeness in the nucleon [21,22]. From the published result on the measured asymmetry of the HAPPEX collaboration [6] at  $Q^2 = 0.477 \text{ (GeV}/c)^2$  and  $\theta_e = 12.3^\circ$ , we recalculated the combination using our parameterization for the electromagnetic form factors [11] and yield  $G_E^s + 0.395G_M^s = 0.034 \pm 0.026$  and  $F_1^s + 0.186F_2^s = 0.024 \pm 0.019$ . Lacking more detailed information, we make the *ad hoc* assumption that  $F_2^s$  in the  $Q^2$  range between 0.1 and 0.5  $(\text{GeV}/c)^2$  can be approximated by  $F_2^s = -0.150 \pm 0.150$ , corresponding to  $G_M^s = -0.099 \pm 0.154$ . This assumption is guided by the fact that this value covers within 2 standard deviations all theoretical estimates as well

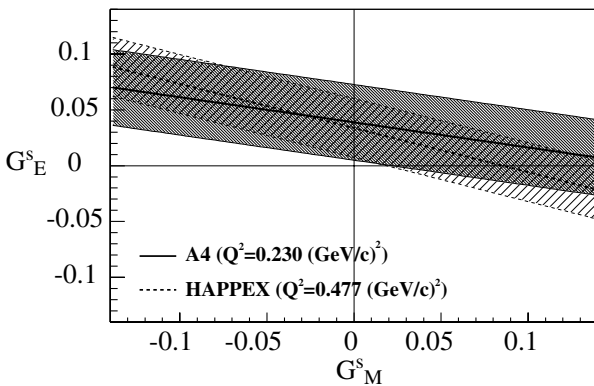


FIG. 3. The solid line represents all possible combinations of  $G_E^s + 0.225G_M^s$  as extracted from the work presented here at a  $Q^2$  of  $0.230 \text{ (GeV}/c)^2$ . The densely hatched region represents the uncertainty. The recalculated result from the HAPPEX published asymmetry at  $Q^2$  of  $0.477 \text{ (GeV}/c)^2$  is indicated by the dashed line; the less densely hatched area represents the associated error of the HAPPEX result.

as the SAMPLE result from Ref. [5]. This yields a value for  $G_E^s$  evaluated from our measurement of  $G_E^s[Q^2 = 0.230 \text{ (GeV}/c)^2] = 0.061 \pm 0.035$  and  $F_1^s[Q^2 = 0.230 \text{ (GeV}/c)^2] = 0.052 \pm 0.034$ . If one makes the further approximation of neglecting the  $Q^2$  dependence in  $G_E^s$ , we can combine our result with the recalculated HAPPEX result by calculating the weighted average, which yields an estimate of  $F_1^s[0.1 \text{ (GeV}/c)^2 < Q^2 < 0.5 \text{ (GeV}/c)^2] = 0.052 \pm 0.024$  and  $G_E^s[0.1 \text{ (GeV}/c)^2 < Q^2 < 0.5 \text{ (GeV}/c)^2] = 0.066 \pm 0.026$ .

The significance level of  $2.2\sigma$  for  $F_1^s$  and  $2.5\sigma$  for  $G_E^s$  that we obtain using the assumption described above leads us to the conclusion that the combination of our measurements presented here with the earlier work of the HAPPEX collaboration shows for the first time evidence for the observation of a contribution of the strange quarks to the electric vector form factor of the nucleon.

This work is supported by the DFG under SFB 201, SPP 1034, by the IN2P3 of CNRS, and in part by the DOE. We are indebted to K. H. Kaiser and the MAMI crew and we thank the A1 Collaboration for the Møller polarimeter measurements.

\*Corresponding author.

Electronic address: maas@kph.uni-mainz.de

- [1] M. G. Olsson *et al.*, PiN Newslett. **16**, 382 (2002).
- [2] D. Adams *et al.*, Phys. Rev. D **56**, 5330 (1997).
- [3] D. H. Beck and B. R. Holstein, Int. J. Mod. Phys. E **10**, 1 (2001).
- [4] A. Silva *et al.*, Nucl. Phys. **A721**, 417 (2003).
- [5] R. Hasty *et al.*, Science **290**, 2117 (2000).
- [6] K. A. Aniol *et al.*, Phys. Lett. B **509**, 211 (2001).
- [7] H. Euteneuer *et al.*, in *Proceedings of the 4th European Particle Accelerator Conference, London, 1994* (World Scientific, Singapore, 1994), p. 506.
- [8] H. Weigel *et al.*, Phys. Lett. B **353**, 20 (1995).
- [9] D. B. Kaplan *et al.*, Nucl. Phys. **B310**, 527 (1988).
- [10] M. Musolf *et al.*, Phys. Rep. **239**, 1 (1994).
- [11] J. Friedrich *et al.*, Eur. Phys. J. A **17**, 607 (2003).
- [12] W. J. Marciano and A. Sirlin, Phys. Rev. D **29**, 75 (1984).
- [13] K. Hagiwara *et al.*, Phys. Rev. D **66**, 010001 (2002).
- [14] S.-L. Zhu *et al.*, Phys. Rev. D **62**, 033008 (2000).
- [15] F. E. Maas *et al.*, Eur. Phys. J. A **17**, 339 (2003).
- [16] K. Aulenbacher *et al.*, Nucl. Instrum. Methods Phys. Res., Sect. A **391**, 498 (1997).
- [17] M. Seidl *et al.*, in *Proceedings of the 7th European Particle Accelerator Conference, Vienna, 2000* (JACoW, 2000), p. 1930 [<http://www.JACoW.org>].
- [18] P. Bartsch, dissertation, Universität Mainz, 2001.
- [19] F. E. Maas *et al.*, *Proceedings of the 7th International Conference on Advanced Technology and Particle Physics* (World Scientific, Singapore, 2002), p. 758.
- [20] P. Achenbach *et al.*, Nucl. Instrum. Methods Phys. Res., Sect. A **465**, 318 (2001).
- [21] R. Jaffe, Phys. Lett. B **229**, 275 (1989).
- [22] H. W. Hammer *et al.*, Phys. Lett. B **367**, 323 (1996).